Environmental Science & Technology

pubs.acs.org/est

Article

Global Perspective of Drought Impacts on Ozone Pollution Episodes

Yadong Lei, Xu Yue,* Hong Liao,* Lin Zhang, Hao Zhou, Chenguang Tian, Cheng Gong, Yimian Ma, Yang Cao, Roger Seco, Thomas Karl, and Mark Potosnak

Cite This: *Environ. Sci. Technol.* 2022, 56, 3932−3940

Read Online

ACCESS | Metrics & More | Article Recommendations | Supporting Information

ABSTRACT: Ozone (O_3) pollution threatens global public health and damages ecosystem productivity. Droughts modulate surface O_3 through meteorological processes and vegetation feedbacks. Unraveling these influences is difficult with traditional chemical transport models. Here, using an atmospheric chemistry−vegetation coupled model in combination with a suite of existing measurements, we investigate the drought impacts on global surface O_3 and explore the main driving processes. Relative to the mean state, accelerated photochemical rates dominate the surface O_3 enhancement during droughts except for eastern U.S. and western Europe, where reduced stomatal uptakes make comparable contributions. During 1990−2012, the simulated frequency of O_3 pollution episodes in western Europe decreases greatly with a negative trend of −5.5 ± 6.6 days per decade following the reductions in anthropogenic emissions if meteorology is fixed. However, such decreased trend is weakened to −2.1 ± 3.8 days per decade, which is closer to the observed trend of −2.9 ± 1.1 days per decade when year-to-year meteorology is applied because increased droughts alone offset 43% of the effects from air pollution control. Our results highlight that more stringent controls of O_3 precursors are necessary to mitigate the higher risks of O_3 pollution episodes by more droughts in a warming world.

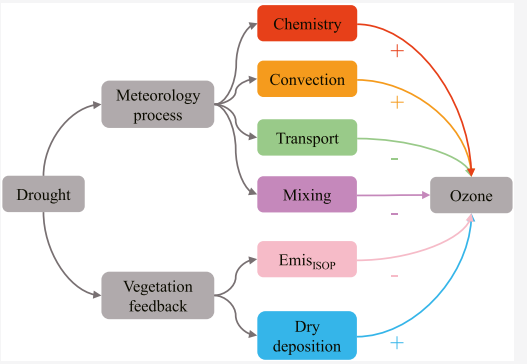

KEYWORDS: *ozone pollution, drought, meteorological processes, vegetation feedbacks, chemistry−vegetation model*

1. INTRODUCTION

Ozone (O_3) pollution is a key concern for global human health and land ecosystems.[1−5] As a secondary pollutant, tropospheric O_3 is primarily formed by the photochemical reactions involving nitrogen oxides ($NO_x \equiv NO + NO_2$) and volatile organic compounds (VOCs) that have both anthropogenic and biogenic sources.[6,7] Meanwhile, O_3 is lost through photolysis in the presence of water vapor and dry deposition to the vegetated surface.[8] The regional O_3 level depends not only on the local chemical production but also on the transboundary transportation.[9] These processes are sensitive to meteorological variables, such as daily maximum temperature, atmospheric relative humidity, and cloud cover fraction.[10−12]

Drought is a recurring climate extreme that has devastating impacts on the ecological environment.[13,14] It can also shape surface O_3 by modulating emissions of biogenic O_3 precursors,[15] chemical production rate,[16] loss rate through dry deposition,[17] and atmospheric transport/mixing.[18] While drought affects surface O_3 through chemical and vegetation processes, it remains a challenge to disentangle these effects mainly because two-way coupling is not adequately represented in most of the terrestrial biosphere models and/or global chemistry models. For example, O_3 dry deposition and biogenic emissions in current chemical transport models usually lack the responses to phenology, CO_2 concentrations, or soil water availability.[19−21]

Here, we examine the impacts of drought on the global trends of O_3 pollution episodes (OPEs) from 1981 to 2015 using a newly developed atmospheric chemistry−vegetation model in combination with a suite of existing measurements (see Section 2). The Yale Interactive terrestrial Biosphere (YIBs) model has been recently coupled with the chemical transport model GEOS-Chem (GC-YIBs) to consider the interactions between atmospheric pollution and land ecosystems.[22] The photosynthesis-dependent stomatal conductance and BVOC emission schemes applied in GC-YIBs reasonably reproduce the observed reductions in both dry deposition and isoprene emissions during droughts. With these updates, we quantify the contributions of various processes (chemistry, isoprene emissions, dry deposition, transport, mixing, and convection) to the changes of O_3 in response to droughts.

Received: October 27, 2021
Revised: March 8, 2022
Accepted: March 8, 2022
Published: March 17, 2022

https://doi.org/10.1021/acs.est.1c07260
Environ. Sci. Technol. 2022, 56, 3932−3940

2. MATERIALS AND METHODS

2.1. Site-Level Measurements. We collected isoprene emission datasets from two field campaigns at the Missouri Ozarks flux (MOFLUX) site in summers 2011[23] and 2012.[24] The MOFLUX site is located in central Missouri (38.74°N, 92.20°W) and dominated by broadleaf deciduous forests. The site experienced a mild drought in the late summer of 2011 and an extreme drought in the summer of 2012. Therefore, this set of data has been widely used to investigate the isoprene changes in response to drought.[15,25]

There are few sites providing observations of the O_3 dry deposition velocity for both dry and wet conditions. Sorting previous publications, we found three sites with available measurements including the Ontario site (44.19°N, 79.56°W) in Canada, the Mea Moh site (18.28°N, 99.72°E) in Thailand, and a former Anglo-Brazilian Amazonian Climate Observation Study (ABRACOS) site (10.1°S, 61.9°W) in southwest Amazon.[26−28] The differences between dry and wet conditions at these sites are used to evaluate the performance of the GC-YIBs model in simulating the response of the O_3 dry deposition velocity to droughts.

Meanwhile, two unprecedented droughts in summer 2012 in Missouri, U.S., and summer 2003 in southwest Europe are selected to evaluate the performance of the GC-YIBs model in simulating the responses of daily maximum 8-h average (MDA8) O_3 concentrations to droughts. We apply quality controls (data available for at least 18 h per day and 26 days per month) to select sites with continuous observations in summers 2011 and 2012 in the state of Missouri, U.S., and summers 2003 and 2004 in southwest Europe. As a result, MDA8 O_3 concentrations are calculated from 18 sites (Table S1, https://www.epa.gov) in Missouri, USA, from Clean Air Status and Trends Network (CASTNET) and 15 sites (Table S2, http://ebas.nilu.no) in southwest Europe from European Monitoring and Evaluation Programme (EMEP). Additionally, measurements from nine sites (Table S3) with continuous records are used to evaluate the simulated O_3 pollution episode trend in western Europe during 1990−2012.

2.2. GC-YIBs Model. GC-YIBs is a coupled global atmospheric chemistry−vegetation model developed by implementing YIBs into GEOS-Chem version 12.1.0.[22] It links atmospheric chemistry and ecosystems in a two-way coupling: the YIBs predicts daily LAI and hourly stomatal conductance for the dry deposition and isoprene emissions in GEOS-Chem v12.1.0; in turn, online-simulated surface O_3 in GEOS-Chem v12.1.0 influences the carbon cycle and plant growth in YIBs. In GC-YIBs, the GEOS-Chem and YIBs models are driven by the same meteorological fields from the MERRA2 reanalysis.[29]

GEOS-Chem is a global three-dimensional (3D) chemical transport model widely used by research groups around the world. It includes fully O_3−NO_x−hydrocarbon−aerosol chemical mechanisms with more than 100 species and 300 reactions.[30,31] Previous studies have evaluated the GEOS-Chem chemical module and found that GEOS-Chem can generally capture the relationship between O_3 and temperature.[32,33] The anthropogenic and biogenic emissions are calculated through the online Harvard NASA Emissions Component (HEMCO) module.[34] Global daily biomass burning emissions apply Global Fire Emissions Database version 4.1 (GFED4.1) inventory from 1997 to 2016.[35] Global anthropogenic emissions inventory is from Emissions Database for Global Atmospheric Research (EDGAR v43, https://edgar.jrc.ec.europa.eu), which provides monthly emissions by multiplying seasonal scaling factors to the annual total emissions. In addition, GEOS-Chem uses some regional inventories, mainly including the EMEP inventory over 1990−2012 in Europe (https://www.emep.int), the NEI inventory over 2006−2013 in USA (https://www.epa.gov), and the MIX inventory over 2008−2010 in Asia (http://www.meicmodel.org). The stomatal uptake in the dry deposition scheme of GEOS-Chem is updated by the online YIBs model[22] (see details in the Supporting Information, SI), while the nonstomatal uptake is still calculated using the Wesely[36] scheme. In GEOS-Chem v12.1.0, the isoprene emission is estimated using the Model of Emissions of Gases and Aerosols from Nature version 2.1 (MEGAN2.1) algorithm.[37] However, recent studies showed that the MEGAN2.1 scheme poorly simulated the changes of isoprene emissions in response to droughts because this scheme applies an empirical algorithm to represent the responses of isoprene emissions to soil moisture (see details in the SI), which is highly dependent on the selection of wilting point.[24,25,38] To reduce uncertainties from isoprene simulation, we couple a photosynthesis-dependent isoprene emission scheme (PS_BVOC, see details and comparisons in the SI) within YIBs into GEOS-Chem to quantify the effects of isoprene changes on surface O_3 under drought conditions.

YIBs is a terrestrial vegetation model developed by Yue and Unger.[39] It can dynamically predict the changes in LAI and tree height through carbon assimilation, respiration, and allocation processes. The model computes plant photosynthesis for nine plant functional types (PFTs) based on the Farquhar et al.[40] and Spitters[41] schemes. The leaf-level stomatal conductance follows the model of Ball and Berry.[42] The LAI and carbon allocation algorithms follow the TRIFFID model.[43] The YIBs model calculates leaf-level isoprene emission using the PS_BVOC scheme, which depends on the photosynthesis rate.[44] The detailed parameter setting of YIBs is well documented in an earlier study.[39]

2.3. O_3 Budget Diagnostic. GEOS-Chem v12.1.0 and later versions apply a mass balanced approach to diagnose the O_3 budget for three column regions, including the troposphere, planetary boundary layer (PBL), and full column (http://wiki.seas.harvard.edu/geos-chem). The O_3 budget is calculated as the difference in vertically integrated column O_3 mass before and after major processes, including chemistry, transport, mixing, convection, and dry deposition. These diagnostics are self-consistent and fully conservative. Thus, the changes in net O_3 production (ΔOP) are driven by six processes, including chemistry (ΔCH), transport (ΔTR), mixing (ΔMI), convection (ΔCO), isoprene emission (ΔIS), and dry deposition (ΔDR): $\Delta OP = \Delta CH + \Delta TR + \Delta MI + \Delta CO + \Delta IS + \Delta DR$.

2.4. Definition of Drought Pentads. For decades, many drought indices were developed for drought assessment,[45−48] such as the standardized precipitation index (SPI), palmer drought severity index (PDSI), and standardized precipitation evapotranspiration index (SPEI). These indices can be calculated on a range of timescales from 1 to 48 months, representing the monthly, seasonal, and interannual changes of dry and wet conditions. However, it is difficult to use these common indices to identify droughts with a duration of less than 1 month.[49,50] Recently, flash droughts have been categorized as a type of climate extreme, which is defined based on the pentad-average daily maximum temperature and

https://doi.org/10.1021/acs.est.1c07260
Environ. Sci. Technol. 2022, 56, 3932−3940

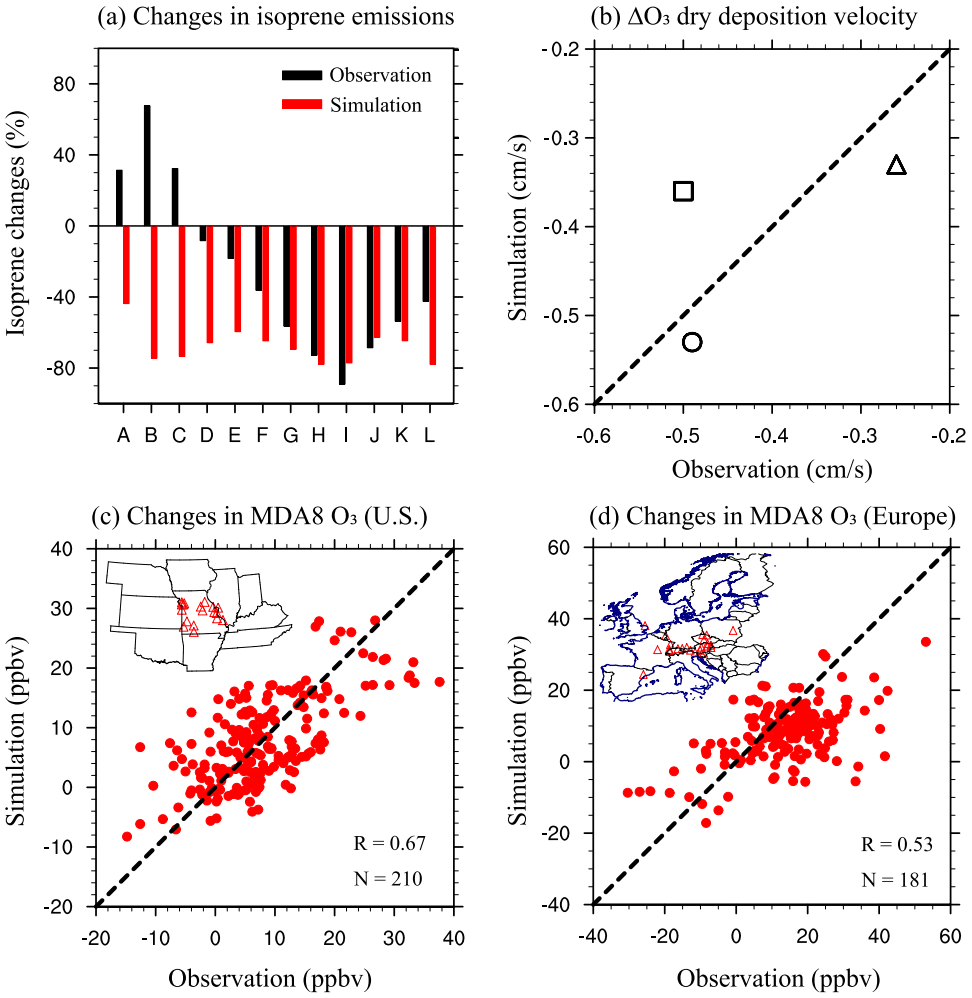

Figure 1. Evaluation of the biogeochemical responses to drought in the GC-YIBs model. (a) Comparison of the relative changes in isoprene emission rates caused by drought (2012 minus 2011) between observation (black) and simulation (red) at site MOFLUX (38.74°N, 92.20°W) using a PS_BVOC scheme. The letters A to L in the X axis represent 12 drought pentads. (b) Comparison between observed and simulated changes in the O_3 dry deposition velocity during droughts at three sites, including the Ontario site (44.19°N, 79.56°W) in Canada (circle, July of 2012 minus July of 2009), the Mea Moh site (10.28°N, 99.72°E) in Thailand (square, January−April minus May−August of 2004), and the ABRACOS site (10.1°S, 61.9°W) in southwest Amazon (triangle, September−October minus May of 1999). (c) Comparison between observed and simulated changes in daily maximum 8-h average (MDA8) O_3 concentrations during the drought pentads in summer 2012 relative to summer 2011 from 18 sites (red triangles in the upper-left corner) in Missouri, U.S. (d) Comparison between observed and simulated MDA8 O_3 from 15 sites (red triangles in the upper-left corner) in response to 2003 summer drought (2003 minus 2004) in southwestern Europe.

soil moisture, representing dry or wet conditions on a submonth scale.[51−55] In this study, we choose flash droughts to investigate the changes of O_3 in response to droughts because our study mainly focuses on O_3 pollution episodes, which usually last 1−7 days.

We focus on the drought events occurring in growing seasons (May−October in the mid-high northern hemisphere, November−April in the mid-high southern hemisphere, and January−December in the tropics).[56] For each year, the seasons are divided into 36 pentads (a pentad includes five days) in the mid-high latitudes but 73 pentads in the tropics. So, we collect 1260 pentads in mid-high and 2555 pentads in low latitudes for all grid cells during 1981−2015. A drought pentad is defined if the pentad-average daily maximum temperature (T_{max}) anomaly is greater than one standard deviation and soil moisture is less than 40th percentile.[51,52] For each grid cell, we define the frequency of drought pentads as the percent of drought pentads in the total number of pentads (N/N_{total}).

2.5. Model Experiments. With the GC-YIBs model, we conduct three simulations to quantify the changes of O_3 production and the frequency of OPEs (MDA8 greater than 95th percentile) in response to drought pentads: (1) FIX is driven with averaged meteorological variables for 1980−2015. To retain the seasonal and diurnal variability, the hourly and 3-hourly variables for each day of the year are averaged through 1980−2015. The reason why we design FIX simulation using averaged meteorology is to avoid drought conditions in some areas if meteorology from a specific year is applied. (2) VAR is driven with year-to-year meteorological variables from 1980 to 2015. (3) VAR_FIX$_{ISOP}$ is the same as the VAR simulation but applies isoprene emissions from the FIX simulation. The time steps in the GC-YIBs model are set to half an hour for dynamic (transport, PBL mixing, cloud convection and wet deposition) and 1 h for chemistry (dry deposition, emissions, and chemistry) processes. Each simulation is driven with meteorological fields from MERRA2 reanalysis with a horizontal resolution of 5 × 4° (longitude by latitude) from

https://doi.org/10.1021/acs.est.1c07260
Environ. Sci. Technol. 2022, 56, 3932−3940

1980 to 2015. The first-year simulation is defined as spin-up, and the simulations from 1981 to 2015 are used for analyses. For selected drought pentads on each grid cell, the differences between VAR and FIX simulations represent O_3 changes in response to drought pentads because both simulations have the same anthropogenic and wildfire emissions. The differences between VAR and VAR_FIX$_{ISOP}$ simulations isolate the impacts of isoprene emissions on O_3 for selected drought pentads.

2.6. Offsetting Effects. In this study, we attempt to quantify the offsetting effects (OFEs) of increased droughts on air pollution control in Europe based on the differences of OPE trends between FIX ($TR_{OPEs,\ FIX}$) and VAR simulations ($TR_{OPEs,\ VAR}$), which include impacts from a wide variety of meteorology. Here, we apply the drought impact factor f to isolate the OFE of drought pentads from other meteorology on air pollution control in Europe: $OFE = [(TR_{OPEs,VAR} - TR_{OPEs,FIX})/TR_{OPEs,\ FIX}] \times f \times 100\%$. In general, the OPEs driven by unfavorable meteorological factors are accompanied by local high temperature or low humidity extremes.[26−28] Thus, we define f simply based on frequencies of OPEs with drought pentads ($OPED_s$) and OPEs with high temperature (daily maximum temperature is greater than one standard deviation) or low humidity (daily relative humidity is lower than one standard deviation) extremes ($OPETH_s$): $f = OPED_s/OPETH_s$ (see calculated f values in the SI). Although this simple definition includes some uncertainties that high temperature or low humidity extremes cannot represent all unfavorable meteorological factors for OPEs, it provides an effective way to explore the offsetting effects associated with only drought pentads.

3. RESULTS

3.1. Model Evaluation. The simulated isoprene emissions, O_3 dry deposition velocities, and MDA8 are evaluated based on site-level measurements (Figures S3−S5). The results show that the GC-YIBs model can generally capture observed isoprene emissions, O_3 dry deposition velocities, and MDA8 with the correlation coefficients of 0.57−0.7 (see details in the SI). To promote the confidence level of this study, the simulated changes in isoprene emissions, O_3 dry deposition velocities, and MDA8 in response to drought are further evaluated.

Site-level measurements have shown that isoprene emissions stay constant or slightly increase at the initial stages of drought but shift to a large reduction at the middle-late stages of drought.[14,15,23,24,57] We evaluate the PS_BVOC scheme in simulating isoprene emissions at the MOFLUX site during drought pentads (Figure 1a). Here, we mainly focus on the relative changes of isoprene emissions in response to drought pentads because both the PS_BVOC and MEGAN2.1 schemes underestimate the magnitude of isoprene emissions (see absolute changes in the SI). The site experienced 13 drought pentads in summer 2012 but only 2 in summer 2011. We select 12 pentads with drought in 2012 but normal conditions in 2011. The isoprene changes in 2012 relative to 2011 during the 12 selected pentads represent the response of isoprene emissions to drought pentads. Observed isoprene emissions remained stable for the first three pentads but then decreased gradually during the remaining nine pentads. Compared to observations, the PS_BVOC scheme reasonably captures the reductions in isoprene emissions during the last nine drought pentads but fails at the first three pentads. The PS_BVOC scheme calculates isoprene emissions based on vegetation photosynthesis, which decreases in response to drought stress. However, laboratory studies showed that nonphotosynthesis carbon pools may dominate the synthesis of isoprene emitted during early or weak drought conditions.[58−60]

Dry deposition regulates the O_3 sink and is sensitive to meteorological variables. We collected existing measurements from three sites across Canada, Thailand, and southwest Amazon to evaluate the responses of the O_3 dry deposition velocity to drought (Figure 1b). Relative to wet conditions, daytime means the O_3 dry deposition velocity decreased by 0.5 cm s^{-1} at the ABRACOS site, 0.49 cm s^{-1} at the Ontario site, and 0.26 cm s^{-1} at the Mea Moh site under dry conditions. Compared to observations, the GC-YIBs model slightly overestimates the reduction of the O_3 dry deposition velocity by 0.04 cm s^{-1} at the Ontario site and 0.07 cm s^{-1} at the Mea Moh site but underestimates it by 0.14 cm s^{-1} at the ABRACOS site.

We further evaluate the simulated MDA8 O_3 in response to severe droughts in Missouri (U.S.) and southwest Europe. Compared to summer 2011, observed MDA8 increases by 7.91 ppbv averaged over 210 drought pentads in summer 2012 in Missouri (Figure 1c). An average increase of 13.5 ppbv in surface O_3 is observed at 181 drought pentads in summer 2003 relative to summer 2004 in southwest Europe (Figure 1d). Compared to observations, simulations predict a similar enhancement of 7.68 ppbv in Missouri with a correlation coefficient of 0.67 ($p < 0.05$). However, the GC-YIBs model predicts a smaller O_3 enhancement of 8.2 ppbv in southwest Europe with a correlation coefficient of 0.53 ($p < 0.05$).

3.2. Attribution of O_3 Changes within the Planetary Boundary Layer. Drought pentads show high frequencies in the tropics but low occurrence in the boreal regions (Figure S6). On the global scale, drought pentads account for 2.6% days (including all grids) on average during 1981−2015, leading to an enhancement (the difference between VAR and FIX simulations during drought pentads) of O_3 by 2.8 ppbv. Regionally, the largest frequency of drought pentads is found in India, which is mainly related to unstable South Asian summer monsoon.[61,62] Additionally, drought pentads account for 15.3% days in central Africa (10°S to 10°N, 10°E to 40°E), 13.7% in Amazon (25°S to 0°, 70°W to 40°W), 9.4% in eastern U.S. (30°N to 44°N, 95°W to 75°W), 7.6% in western Europe (40°N to 60°N, 0° to 50°E), and 7.3% in eastern China (22°N to 46°N, 105°E to 122.5°E). The more frequent drought pentads increase regional O_3 by 5.5 ppbv in eastern U.S., 3.5 ppbv in eastern China, 6.5 ppbv in western Europe, 2.7 ppbv in Amazon, and 1.8 ppbv in central Africa (Figure S7).

Based on the changes of the O_3 budget in VAR simulation relative to FIX simulation, we further quantify the contributions of six processes, including chemistry, isoprene emissions, dry deposition, convection, mixing, and transport, to the O_3 anomaly during drought pentads (Figures 2 and S8). Overall, the changes in chemistry, reductions in dry deposition, and increases in convection processes increase O_3, while the decreased isoprene emissions and increased mixing and transport processes reduce O_3 during drought pentads. Except in western Europe, the largest positive contribution is from the chemical process, which increases O_3 by 1.78 Gg/day in eastern U.S., 1.56 Gg/day in eastern China, 1.2 Gg/day in Amazon, and 1.1 Gg/day in central Africa. Increased soil NO_x emissions (Figure S9d) under drought pentads promote the

https://doi.org/10.1021/acs.est.1c07260
Environ. Sci. Technol. 2022, 56, 3932−3940

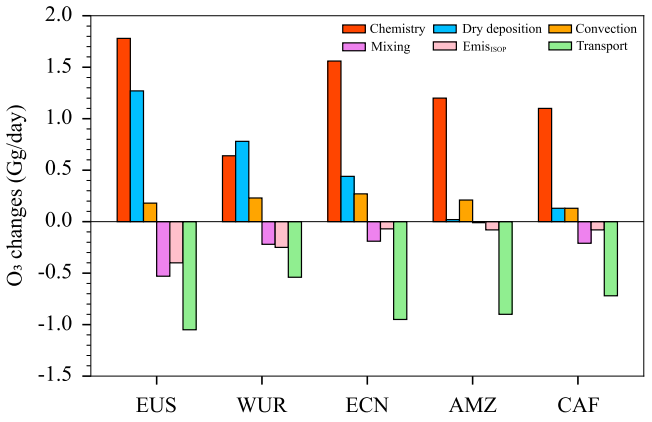

Figure 2. Attribution of drought-induced changes in O_3 within the planetary boundary layer using the changes of O_3 budget in VAR simulation relative to FIX simulation during drought pentads. The contributions of six processes to the O_3 anomaly in eastern U.S. (EUS), western Europe (WUR), eastern China (ECN), Amazon (AMZ), and central Africa (CAF) are shown for drought pentads. The red, blue, orange, violet, pink, and green colors represent contributions by chemistry, dry deposition, convection, mixing, isoprene emissions, and transport processes, respectively.

concentrations of O_3 precursors. Additionally, the drought-induced enhancement in T_{max} (Figure S9a) and reduction in atmospheric relative humidity (Figure S9b) accelerate photochemical reaction rates,[12,63,64] resulting in large increases of O_3 in high oxidizing environments. For the Amazon and central Africa, where anthropogenic emissions are low, frequent wildfires promote ambient concentrations of precursors, making these regions sensitive to drought pentads (Figure S10b).

Dry deposition also makes important contributions to the O_3 anomaly. Such contributions show comparable magnitude to the chemistry processes in eastern U.S. and western Europe, where dry deposition, respectively, increases to O_3 by 1.27 and 0.78 Gg/day. During drought pentads, plants reduce stomatal conductance to prevent water loss (Figure S9e). Such physiological response inhibits O_3 dry deposition (Figure S9f), leading to enhanced O_3. It should be noted that there are limited changes in the O_3 dry deposition velocity under drought pentads in the tropics despite the changes of stomatal conductance are comparable with those in mid-high latitudes. This discrepancy may be attributed to moderate meteorological anomaly (Figure S9a,b) during drought pentads caused by the smaller interannual variability of climate in the tropics. Additionally, decreased isoprene emissions (Figure S2d) reduce O_3 by 0.4 Gg/day in eastern U.S., 0.25 Gg/day in western Europe, 0.07 Gg/day in eastern China, and 0.08 Gg/day in central Africa.

Transport processes in the GC-YIBs model represent O_3 advection in the vertical and horizontal directions, which is influenced by large-scale circulation anomalies. During drought pentads, anomalous downdraft and diverging flows related to high-pressure systems enhance O_3 horizontal transport. For these regions, transport processes reduce O_3 by 1.05 Gg/day in eastern U.S., 0.54 Gg/day in western Europe, 0.95 Gg/day in eastern China, 0.9 Gg/day in Amazon, and 0.72 Gg/day in central Africa. Such magnitude of changes is secondary to chemical processes but with opposite signs. Mixing processes in the PBL represent the O_3 exchange between the PBL and the free troposphere. Increased PBL height (Figure S9c) under drought pentads enhances O_3 upward mixing from the PBL to the free troposphere, leading to reductions in surface O_3 by 0.53 Gg/day in eastern U.S., 0.22 Gg/day in western Europe, 0.19 Gg/day in eastern China, and 0.21 Gg/day in central Africa. Additionally, drought pentads inhibit the development of cloud convection, which increases O_3 by 0.18 Gg/day in eastern U.S., 0.23 Gg/day in western Europe, 0.27 Gg/day in eastern China, 0.21 Gg/day in Amazon, and 0.13 Gg/day in central Africa.

3.3. Consequences and Implications. OPEs are often accompanied by drought pentads (Figure S11). Here, we use a co-occurrence frequency ratio (CF_{OD}) to investigate the dependence of OPEs on drought pentads. CF_{OD} is defined as the ratio between the frequency of OPEs with drought pentads ($OPED_s$) and the frequency of all OPEs:

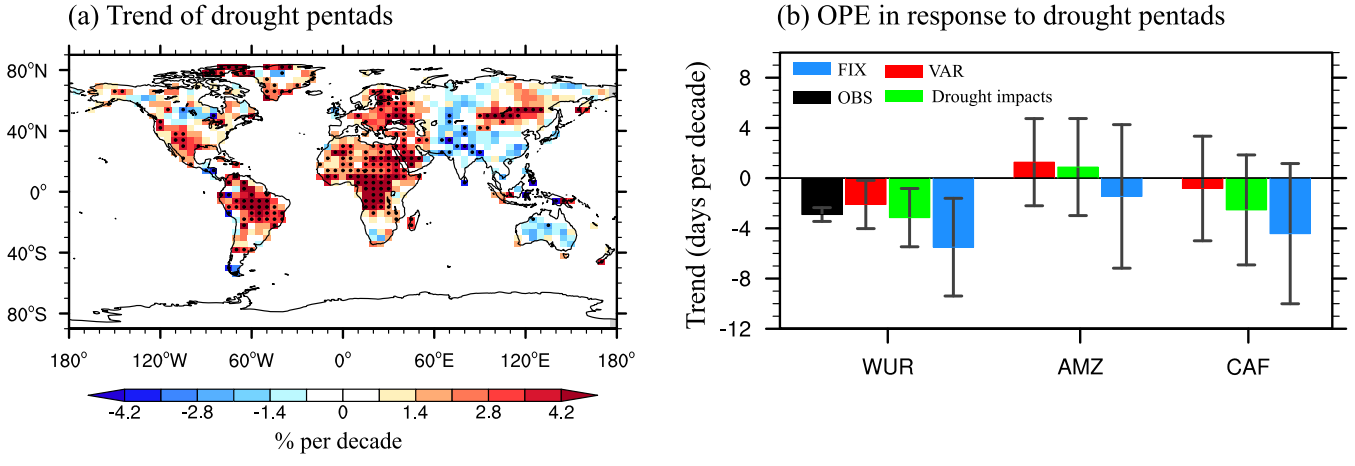

Figure 3. Impacts of drought pentads on O_3 pollution episodes. (a) Linear trends of the drought pentads per year during 1981−2015. The black dots indicate statistically significant changes ($p < 0.01$). (b) Linear trends of O_3 pollution episodes (OPEs) occurrence in western Europe (WUR, 1990−2012), Amazon (AMZ, 1997−2015), and central Africa (CAF, 1997−2015). The positive (negative) value represents that OPEs become more (less) frequent. The black bar in panel (b) represents observed OPE trends in western Europe calculated using long-term measurements at nine sites (Table S3). The blue and red bars represent OPE trends in FIX and VAR simulations, respectively. The green bars represent OPE trends separated by the drought impact factor (details in SI). The black error bars represent the one standard deviation of grids.

https://doi.org/10.1021/acs.est.1c07260
Environ. Sci. Technol. 2022, 56, 3932−3940

$CF_{OD} = \frac{OPED_s}{OPE_s} \times 100\%$. The strong dependence of OPEs on drought pentads is found in the U.S., western Europe, central Africa, and Amazon, where $OPED_s$ can account for 46, 55, 45, and 67% of the OPEs, respectively. In eastern China, $OPED_s$ only account for 30% of the OPEs, indicating the importance of anthropogenic emissions and other weather extremes on OPEs.

A positive trend of drought pentads influences the regional tendency of OPEs. Since 1980, OPEs showed limited reductions in Europe,[17] despite the large decline of chemical precursors for NO_x (50%, Figure S10c) and nonmethane VOCs (67%).[65] Meanwhile, drought pentads increased by 1.8% per decade in western Europe from 1981 to 2015 (Figure 3a), which is mainly attributed to increased heatwave occurrence (Figure S12a). Following the reductions in O_3 precursors, the frequency of OPEs decreases greatly during 1990−2012 with a negative trend of −5.5 ± 6.6 days per decade if fixed meteorology (FIX) is used. However, such decreased trend is weakened to −2.1 ± 3.8 days per decade if the simulation is driven by year-to-year meteorology (VAR), which is close to the observed trend of −2.9 ± 1.1 days per decade (Figures 3b and S13). Furthermore, we separate the impacts of drought pentads from climate change on OPEs based on the drought impact factor f (see details in Section 2.6). Considering the impacts of increased drought pentads alone, the frequency of OPEs shows a trend of −3.1 ± 4.6 days per decade during 1990−2012, suggesting that increased drought pentads offset 43% of the effects from air pollution control policy over past 23 years (see methods in Section 2.5). Similar conclusions were achieved by an earlier study,[17] which attributed the changes of OPEs in Europe mainly to the weakened vegetation feedback during droughts. Our results highlight that the effects of chemical processes show comparable magnitude to the reduced dry deposition in Europe but outweigh the effects of dry deposition changes elsewhere globally (Figure 2).

Amazon and central Africa also suffer increased drought pentads in the past three decades due to decreased rainfall (Figures 3a and S12b). In contrast to Europe, the formation of surface O_3 in these two regions is dominated by natural emissions from wildfires.[66] For central Africa, the frequency of OPEs decreases by −4.4 ± 11.2 days per decade from 1997 to 2005 in FIX simulation, following reduced O_3 precursors generated by wildfires ($p < 0.01$, Figure S10d). As considering the impacts of increased drought pentads alone in meteorology, such decreased trend is weakened to −2.5 ± 8.7 days per decade. Similarly, increased drought pentads (3.1% per decade) turn the decreased OPE frequency with a negative trend of −1.5 ± 11.4 days per decade to the increased OPE frequency with a positive trend of 0.9 ± 7.7 days per decade from 1997 to 2015 (Figure 3b). These results show that increased drought pentads either exacerbate O_3 pollution or hinder the recovery of air quality.

4. UNCERTAINTIES

The simulated effects of dry deposition on surface O_3 in the tropics are generally smaller than those in the mid-high latitudes. This discrepancy may be attributable to two aspects: (1) Compared with the mid-high latitudes, the smaller interannual variability of climate in the tropics results in moderate meteorological anomaly during drought pentads (Figure S9), leading to limited effects on vegetation during drought pentads. (2) The GC-YIBs model slightly underestimates the changes of O_3 dry deposition in response to droughts in the tropics (Figure 1b).

There are some uncertainties in simulated O_3 and the associated processes. For isoprene emissions, the PS_BVOC scheme shows lower correlations than MEGAN v2.1 for the global evaluations (Figure S3), but it reasonably captures the inhibition effects of drought on isoprene emissions at the MOFLUX site (Figure 1). Both schemes underestimate the magnitude and variability of isoprene emissions (Figure S1). However, such underestimation may have limited impacts on the main conclusions as attributions showed that isoprene is, in general, a small driver of changes in surface O_3 across regions during drought pentads (Figure 2). For O_3 dry deposition, this study uses a photosynthesis-based stomatal scheme. Although simulated dry deposition velocities are underestimated at some sites (Figure S4), this scheme improves the simulated O_3 dry deposition velocities for major tree species[22] due to consideration of more ecophysiological responses to environmental factors. For surface O_3, although GC-YIBs overestimates the mean level of surface O_3 (Figure S5), it, in general, reproduces the observed O_3 changes between drought and normal periods (Figure 1c,d).

The model simulations in this study are limited to a low resolution (4 × 5°) due to the high computational costs of running integrations more than 30 years. The low resolution will induce uncertainties on surface O_3 simulation. The comparison results of 2011 show that a high resolution of 2 × 2.5° improved the simulated surface O_3 in the U.S. and Europe compared to a low resolution of 4 × 5°, with a higher correlation coefficient (0.68 vs 0.55) and lower root-mean-square error (10.7 vs 11.8) (Figure S14). Similarly, the high resolution also improved the simulated O_3 dry deposition velocity (Figure S15) and isoprene emissions (Figure S16) on local sites due to its finer land cover and more accurate meteorological parameters. However, those comparisons, in general, show consistent features between the simulation with low and high resolutions, suggesting that the relatively coarse spatial resolution applied in this study may not change the main conclusions achieved.

In this study, we set O_3 simulated with averaged meteorology through 1980−2015 as a baseline to explore the effects of droughts on O_3. The reason why we use averaged meteorology is to avoid drought conditions in some areas if meteorology from a specific year is applied. However, such an approach may cause the loss of some nonlinear variabilities in meteorology during the averaging process. As a check, we performed an additional experiment with fixed meteorological forcing in the year 1980. In this new run, similar offsetting effects (32%) of increased droughts on air pollution control policy in western Europe during 1990−2012 were achieved (Figure S17).

Despite these uncertainties, our results reveal that increased drought pentads either exacerbate O_3 pollution or hinder the recovery of air quality. Considering the increased drought pentads in a warming world, our study highlights that more stringent controls to both CO_2 and O_3 precursors are beneficial for mitigating drought risks and improving O_3 air quality in the future.

https://doi.org/10.1021/acs.est.1c07260
Environ. Sci. Technol. 2022, 56, 3932−3940

■ ASSOCIATED CONTENT

Supporting Information

The Supporting Information is available free of charge at https://pubs.acs.org/doi/10.1021/acs.est.1c07260.

Responses of isoprene emissions to drought pentads (Figure S1); global responses of isoprene emissions to drought pentads (Figure S2); evaluation of simulated isoprene emissions (Figure S3); evaluation of simulated O_3 dry deposition velocities (Figure S4); evaluation of simulated surface O_3 (Figure S5); frequencies of drought pentads (Figure S6); changes of O_3 in response to drought pentads (Figure S7); attribution of drought-induced changes in global net O_3 production (Figure S8); global responses of meteorological, biophysical, and biogeochemical variables to drought pentads (Figure S9); spatial and temporal variability of NO_x emissions (Figure S10); co-occurrence of OPEs and drought pentads (Figure S11); linear trends of the drought pentads (Figure S12); difference of OPE trends between VAR and FIX simulations (Figure S13); comparison of simulated surface O_3 between low and high resolutions (Figure S14); comparison of simulated O_3 dry deposition velocities between low and high resolutions (Figure S15); comparison of simulated isoprene emissions between low and high resolutions (Figure S16); and simulated OPE response to drought pentads using fixed meteorology in the year of 1980 (Figure S17) (PDF)

■ AUTHOR INFORMATION

Corresponding Authors

Xu Yue − *Jiangsu Key Laboratory of Atmospheric Environment Monitoring and Pollution Control, Jiangsu Collaborative Innovation Center of Atmospheric Environment and Equipment Technology, School of Environmental Science and Engineering, Nanjing University of Information Science & Technology (NUIST), Nanjing 210044, China;* orcid.org/0000-0002-8861-8192; Email: yuexu@nuist.edu.cn

Hong Liao − *Jiangsu Key Laboratory of Atmospheric Environment Monitoring and Pollution Control, Jiangsu Collaborative Innovation Center of Atmospheric Environment and Equipment Technology, School of Environmental Science and Engineering, Nanjing University of Information Science & Technology (NUIST), Nanjing 210044, China;* Email: hongliao@nuist.edu.cn

Authors

Yadong Lei − *State Key Laboratory of Severe Weather & Key Laboratory of Atmospheric Chemistry of CMA, Chinese Academy of Meteorological Sciences, Beijing 100081, China*

Lin Zhang − *Laboratory for Climate and Ocean-Atmosphere Studies, Department of Atmospheric and Oceanic Sciences, School of Physics, Peking University, Beijing 100871, China;* orcid.org/0000-0003-2383-8431

Hao Zhou − *Climate Change Research Center, Institute of Atmospheric Physics, Chinese Academy of Sciences, Beijing 100029, China; University of Chinese Academy of Sciences, Beijing 100029, China*

Chenguang Tian − *Climate Change Research Center, Institute of Atmospheric Physics, Chinese Academy of Sciences, Beijing 100029, China; University of Chinese Academy of Sciences, Beijing 100029, China*

Cheng Gong − *University of Chinese Academy of Sciences, Beijing 100029, China; State Key Laboratory of Atmospheric Boundary Layer Physics and Atmospheric Chemistry (LAPC), Institute of Atmospheric Physics, Chinese Academy of Sciences, Beijing 100029, China*

Yimian Ma − *Climate Change Research Center, Institute of Atmospheric Physics, Chinese Academy of Sciences, Beijing 100029, China; University of Chinese Academy of Sciences, Beijing 100029, China*

Yang Cao − *Climate Change Research Center, Institute of Atmospheric Physics, Chinese Academy of Sciences, Beijing 100029, China; University of Chinese Academy of Sciences, Beijing 100029, China*

Roger Seco − *Institute of Environmental Assessment and Water Research (IDAEA-CSIC), Barcelona 08034 Catalonia, Spain;* orcid.org/0000-0002-2078-9956

Thomas Karl − *Department of Atmospheric and Cryospheric Sciences, University of Innsbruck, Innsbruck A-6020, Austria*

Mark Potosnak − *Department of Environmental Science and Studies, DePaul University, Chicago, Illinois 60614, United States*

Complete contact information is available at: https://pubs.acs.org/10.1021/acs.est.1c07260

Author Contributions

X.Y., Y.L., and H.L. designed the study. Y.L. conducted the model simulations. Y.L., X.Y., and H.L. analyzed the results. L.Z., H.Z., C.T., C.G., Y.M., Y.C., R.S., T.K., and M.P. revised and improved the manuscript.

Notes

The authors declare no competing financial interest.

The site-level ozone measurements in the U.S. and Europe can be downloaded from https://www.epa.gov and http://ebas.nilu.no, respectively. The isoprene emission datasets at the Missouri Ozarks flux (MOFLUX) site in summer 2011 and 2012 are taken from Potosnak et al.[23] and Seco et al.,[24] respectively. The observed dry deposition velocities of O_3 in 2009 and 2012 are from an earlier study.[26] The source codes for GC-YIBs are available at https://doi.org/10.5281/zenodo.3993832.

■ ACKNOWLEDGMENTS

This work was jointly supported by the National Natural Science Foundation of China (grant no. 41975155) and Jiangsu Science Fund for Distinguished Young Scholars (grant no. BK20200040). R.S. acknowledges grants RYC2020-029216-I and CEX2018-000794-S funded by MCIN/AEI/10.13039/501100011033 and by "ESF Investing in your future". We would like to thank the editor and four anonymous reviewers for their constructive comments which helped improve the quality of the paper.

■ REFERENCES

(1) Lelieveld, J.; Evans, J. S.; Fnais, M.; Giannadaki, D.; Pozzer, A. The contribution of outdoor air pollution sources to premature mortality on a global scale. *Nature* **2015**, *525*, 367−371.

(2) Unger, N.; Zheng, Y.; Yue, X.; Harper, K. L. Mitigation of ozone damage to the world's land ecosystems by source sector. *Nat. Clim. Change* **2020**, *10*, 134−137.

(3) Dang, R.; Liao, H. Radiative Forcing and Health Impact of Aerosols and Ozone in China as the Consequence of Clean Air Actions over 2012−2017. *Geophys. Res. Lett.* **2019**, *46*, 12511−12519.
(4) Dedoussi, I. C.; Eastham, S. D.; Monier, E.; Barrett, S. R. H. Premature mortality related to United States cross-state air pollution. *Nature* **2020**, *578*, 261−265.
(5) Yue, X.; Unger, N.; Harper, K.; Xia, X.; Liao, H.; Zhu, T.; Xiao, J.; Feng, Z.; Li, J. Ozone and haze pollution weakens net primary productivity in China. *Atmos. Chem. Phys.* **2017**, *17*, 6073−6089.
(6) Sillman, S. The relation between ozone, NOx and hydrocarbons in urban and polluted rural environments. *Atmos. Environ.* **1999**, *33*, 1821−1845.
(7) Wang, P.; Chen, Y.; Hu, J.; Zhang, H.; Ying, Q. Attribution of Tropospheric Ozone to NOx and VOC Emissions: Considering Ozone Formation in the Transition Regime. *Environ. Sci. Technol.* **2019**, *53*, 1404−1412.
(8) Lelieveld, J.; Dentener, F. J. What controls tropospheric ozone? *J. Geophys. Res.: Atmos.* **2000**, *105*, 3531−3551.
(9) Gong, C.; Liao, H.; Zhang, L.; Yue, X.; Dang, R.; Yang, Y. Persistent ozone pollution episodes in North China exacerbated by regional transport. *Environ. Pollut.* **2020**, *265*, No. 115056.
(10) Lu, X.; Zhang, L.; Shen, L. Meteorology and Climate Influences on Tropospheric Ozone: a Review of Natural Sources, Chemistry, and Transport Patterns. *Curr. Pollut. Rep.* **2019**, *5*, 238−260.
(11) Jacob, D. J.; Winner, D. A. Effect of climate change on air quality. *Atmos. Environ.* **2009**, *43*, 51−63.
(12) Kavassalis, S.; Murphy, J. G. Understanding ozone-meteorology correlations: A role for dry deposition. *Geophys. Res. Lett.* **2017**, *44*, 2922−2931.
(13) Ciais, P.; Reichstein, M.; Viovy, N.; Granier, A.; Ogee, J.; Allard, V.; Aubinet, M.; Buchmann, N.; Bernhofer, C.; Carrara, A.; et al. Europe-wide reduction in primary productivity caused by the heat and drought in 2003. *Nature* **2005**, *437*, 529−533.
(14) Demetillo, M. A. G.; Anderson, J. F.; Geddes, J. A.; Yang, X.; Najacht, E. Y.; Herrera, S. A.; Kabasares, K. M.; Kotsakis, A. E.; Lerdau, M. T.; Pusede, S. E. Observing Severe Drought Influences on Ozone Air Pollution in California. *Environ. Sci. Technol.* **2019**, *53*, 4695−4706.
(15) Zheng, Y.; Unger, N.; Tadić, J. M.; Seco, R.; Guenther, A. B.; Barkley, M. P.; Potosnak, M. J.; Murray, L. T.; Michalak, A. M.; Qiu, X.; Kim, S.; Karl, T.; Gu, L.; Pallardy, S. G. Drought impacts on photosynthesis, isoprene emission and atmospheric formaldehyde in a mid-latitude forest. *Atmos. Environ.* **2017**, *167*, 190−201.
(16) Rasmussen, D. J.; Fiore, A. M.; Naik, V.; Horowitz, L. W.; McGinnis, S. J.; Schultz, M. G. Surface ozone-temperature relationships in the eastern US: A monthly climatology for evaluating chemistry-climate models. *Atmos. Environ.* **2012**, *47*, 142−153.
(17) Lin, M.; Horowitz, L. W.; Xie, Y.; Paulot, F.; Malyshev, S.; Shevliakova, E.; Finco, A.; Gerosa, G.; Kubistin, D.; Pilegaard, K. Vegetation feedbacks during drought exacerbate ozone air pollution extremes in Europe. *Nat. Clim. Change* **2020**, *10*, 444−451.
(18) Gong, C.; Liao, H. A typical weather pattern for ozone pollution events in North China. *Atmos. Chem. Phys.* **2019**, *19*, 13725−13740.
(19) Hardacre, C.; Wild, O.; Emberson, L. An evaluation of ozone dry deposition in global scale chemistry climate models. *Atmos. Chem. Phys.* **2015**, *15*, 6419−6436.
(20) Silva, S. J.; Heald, C. L. Investigating Dry Deposition of Ozone to Vegetation. *J. Geophys. Res.: Atmos.* **2018**, *123*, 559−573.
(21) Rydsaa, J. H.; Stordal, F.; Gerosa, G.; Finco, A.; Hodnebrog, Ø. Evaluating stomatal ozone fluxes in WRF-Chem: Comparing ozone uptake in Mediterranean ecosystems. *Atmos. Environ.* **2016**, *143*, 237−248.
(22) Lei, Y.; Yue, X.; Liao, H.; Gong, C.; Zhang, L. Implementation of Yale Interactive terrestrial Biosphere model v1.0 into GEOS-Chem v12.0.0: a tool for biosphere−chemistry interactions. *Geosci. Model Dev.* **2020**, *13*, 1137−1153.
(23) Potosnak, M. J.; LeStourgeon, L.; Pallardy, S. G.; Hosman, K. P.; Gu, L.; Karl, T.; Geron, C.; Guenther, A. B. Observed and modeled ecosystem isoprene fluxes from an oak-dominated temperate forest and the influence of drought stress. *Atmos. Environ.* **2014**, *84*, 314−322.
(24) Seco, R.; Karl, T.; Guenther, A.; Hosman, K. P.; Pallardy, S. G.; Gu, L.; Geron, C.; Harley, P.; Kim, S. Ecosystem-scale volatile organic compound fluxes during an extreme drought in a broadleaf temperate forest of the Missouri Ozarks (central USA). *Glob. Change Biol.* **2015**, *21*, 3657−3674.
(25) Jiang, X.; Guenther, A.; Potosnak, M.; Geron, C.; Seco, R.; Karl, T.; Kim, S.; Gu, L.; Pallardy, S. Isoprene Emission Response to Drought and the Impact on Global Atmospheric Chemistry. *Atmos. Environ.* **2018**, *183*, 69−83.
(26) Lin, M.; Malyshev, S.; Shevliakova, E.; Paulot, F.; Horowitz, L. W.; Fares, S.; Mikkelsen, T. N.; Zhang, L. Sensitivity of Ozone Dry Deposition to Ecosystem-Atmosphere Interactions: A Critical Appraisal of Observations and Simulations. *Global Biogeochem. Cycles* **2019**, *33*, 1264−1288.
(27) Matsuda, K.; Watanabe, I.; Wingpud, V.; Theramongkol, P.; Ohizumi, T. Deposition velocity of O-3 and SO2 in the dry and wet season above a tropical forest in northern Thailand. *Atmos. Environ.* **2006**, *40*, 7557−7564.
(28) Rummel, U.; Ammann, C.; Kirkman, G. A.; Moura, M. A. L.; Foken, T.; Andreae, M. O.; Meixner, F. X. Seasonal variation of ozone deposition to a tropical rain forest in southwest Amazonia. *Atmos. Chem. Phys.* **2007**, *7*, 5415−5435.
(29) Gelaro, R.; McCarty, W.; Suarez, M. J.; Todling, R.; Molod, A.; Takacs, L.; Randles, C.; Darmenov, A.; Bosilovich, M. G.; Reichle, R.; Wargan, K.; Coy, L.; Cullather, R.; Draper, C.; Akella, S.; Buchard, V.; Conaty, A.; da Silva, A.; Gu, W.; Kim, G. K.; Koster, R.; Lucchesi, R.; Merkova, D.; Nielsen, J. E.; Partyka, G.; Pawson, S.; Putman, W.; Rienecker, M.; Schubert, S. D.; Sienkiewicz, M.; Zhao, B. The Modern-Era Retrospective Analysis for Research and Applications, Version 2 (MERRA-2). *J. Clim.* **2017**, *30*, 5419−5454.
(30) Park, R. J. Natural and transboundary pollution influences on sulfate-nitrate-ammonium aerosols in the United States: Implications for policy. *J. Geophys. Res.* **2004**, *109*, No. 004473.
(31) Barret, B.; Sauvage, B.; Bennouna, Y.; Le Flochmoen, E. Upper-tropospheric CO and O_3 budget during the Asian summer monsoon. *Atmos. Chem. Phys.* **2016**, *16*, 9129−9147.
(32) Porter, W. C.; Heald, C. L. The mechanisms and meteorological drivers of the summertime ozone−temperature relationship. *Atmos. Chem. Phys.* **2019**, *19*, 13367−13381.
(33) Hu, L.; Keller, C. A.; Long, M. S.; Sherwen, T.; Auer, B.; Da Silva, A.; Nielsen, J. E.; Pawson, S.; Thompson, M. A.; Trayanov, A. L.; Travis, K. R.; Grange, S. K.; Evans, M. J.; Jacob, D. J. Global simulation of tropospheric chemistry at 12.5 km resolution: performance and evaluation of the GEOS-Chem chemical module (v10-1) within the NASA GEOS Earth system model (GEOS-5 ESM). *Geosci. Model Dev.* **2018**, *11*, 4603−4620.
(34) Keller, C. A.; Long, M. S.; Yantosca, R. M.; Da Silva, A. M.; Pawson, S.; Jacob, D. J. HEMCO v1.0: a versatile, ESMF-compliant component for calculating emissions in atmospheric models. *Geosci. Model Dev.* **2014**, *7*, 1409−1417.
(35) van der Werf, G. R.; Randerson, J. T.; Giglio, L.; van Leeuwen, T. T.; Chen, Y.; Rogers, B. M.; Mu, M.; van Marle, M. J. E.; Morton, D. C.; Collatz, G. J.; Yokelson, R. J.; Kasibhatla, P. S. Global fire emissions estimates during 1997−2016. *Earth Syst. Sci. Data* **2017**, *9*, 697−720.
(36) Wesely, M. L. Parameterization of surface resistances to gaseous dry deposition in regional-scale numerical models. *Atmos. Environ.* **1989**, *41*, 52−63.
(37) Guenther, A. B.; Jiang, X.; Heald, C. L.; Sakulyanontvittaya, T.; Duhl, T.; Emmons, L. K.; Wang, X. The Model of Emissions of Gases and Aerosols from Nature version 2.1 (MEGAN2.1): an extended and updated framework for modeling biogenic emissions. *Geosci. Model Dev.* **2012**, *5*, 1471−1492.
(38) Huang, L.; Mcgaughey, G.; Mcdonald-Buller, E.; Kimura, Y.; Allen, D. T. Quantifying regional, seasonal and interannual contributions of environmental factors on isoprene and monoterpene

https://doi.org/10.1021/acs.est.1c07260
Environ. Sci. Technol. 2022, 56, 3932−3940

emissions estimates over eastern Texas. *Atmos. Environ.* **2015**, *106*, 120−128.
(39) Yue, X.; Unger, N. The Yale Interactive terrestrial Biosphere model version 1.0: description, evaluation and implementation into NASA GISS ModelE2. *Geosci. Model Dev.* **2015**, *8*, 2399−2417.
(40) Farquhar, G. D.; Caemmerer, S.; Berry, J. A. A biochemical model of photosynthetic CO2 assimilation in leaves of C3 species. *Planta* **1980**, *149*, 78−90.
(41) Spitters, C. Separating the diffuse and direct component of global radiation and its implications for modeling canopy photosynthe sis Part II—Calculation of canopy photosynthesis. *Agric. For. Meteorol.* **1986**, *38*, 231−242.
(42) Baldocchi, D. D.; Hicks, B. B.; Camara, P. A canopy stomatal resistance model for gaseous deposition to vegetated surfaces. *Atmos. Environ.* **1987**, *21*, 91−101.
(43) Clark, D. B.; Mercado, L. M.; Sitch, S.; Jones, C. D.; Gedney, N.; Best, M. J.; Pryor, M.; Rooney, G. G.; Essery, R. L. H.; Blyth, E.; et al. The Joint UK Land Environment Simulator (JULES), model description—Part 2: Carbon fluxes and vegetation dynamics. *Geosci. Model Dev.* **2011**, *4*, 701−722.
(44) Unger, N. Isoprene emission variability through the twentieth century. *J. Geophys. Res.: Atmos.* **2013**, *118*, 13606−13613.
(45) Dai, A.; Trenberth, K. E.; Qian, T. T. A global dataset of Palmer Drought Severity Index for 1870-2002: Relationship with soil moisture and effects of surface warming. *J. Hydrometeorol.* **2004**, *5*, 1117−1130.
(46) Yue, X.; Tian, C.; Lei, Y. Relieved drought in China under a low emission pathway to 1.5 °C global warming. *Int. J. Climatol.* **2020**, *41*, E259−E270.
(47) Trenberth, K. E.; Dai, A. G.; van der Schrier, G.; Jones, P. D.; Barichivich, J.; Briffa, K. R.; Sheffield, J. Global warming and changes in drought. *Nat. Clim. Change* **2014**, *4*, 17−22.
(48) Naumann, G.; Alfieri, L.; Wyser, K.; Mentaschi, L.; Betts, R. A.; Carrao, H.; Spinoni, J.; Vogt, J.; Feyen, L. Global Changes in Drought Conditions Under Different Levels of Warming. *Geophys. Res. Lett.* **2018**, *45*, 3285−3296.
(49) van der Schrier, G.; Jones, P. D.; Briffa, K. R. The sensitivity of the PDSI to the Thornthwaite and Penman-Monteith parameterizations for potential evapotranspiration. *J. Geophys. Res.: Atmos.* **2011**, *116*, No. 015001.
(50) Vicente-Serrano, S. M.; Begueria, S.; Lopez-Moreno, J. I. A Multiscalar Drought Index Sensitive to Global Warming: The Standardized Precipitation Evapotranspiration Index. *J. Clim.* **2010**, *23*, 1696−1718.
(51) Mo, K. C.; Lettenmaier, D. P. Heat wave flash droughts in decline. *Geophys. Res. Lett.* **2015**, *42*, 2823−2829.
(52) Zhang, Y.; You, Q.; Chen, C.; Li, X. Flash droughts in a typical humid and subtropical basin: A case study in the Gan River Basin, China. *J. Hydrol.* **2017**, *551*, 162−176.
(53) Yuan, X.; Wang, L. Y.; Wood, E. F. Anthropogenic Intensification of Southern African Flash Droughts as Exemplified by the 2015/16 Season. *Bull. Am. Meteorol. Soc.* **2018**, *99*, S86−S90.
(54) Mo, K. C.; Lettenmaier, D. P. Precipitation Deficit Flash Droughts over the United States. *J Hydrometeorol* **2016**, *17*, 1169−1184.
(55) Wang, L. Y.; Yuan, X.; Xie, Z. H.; Wu, P. L.; Li, Y. H. Increasing flash droughts over China during the recent global warming hiatus. *Sci. Rep.* **2016**, *6*, No. 30571.
(56) Hunt, E. D.; Hubbard, K. G.; Wilhite, D. A.; Arkebauer, T. J.; Dutcher, A. L. The development and evaluation of a soil moisture index. *Int. J. Climatol.* **2009**, *29*, 747−759.
(57) Pegoraro, E.; Rey, A.; Greenberg, J. P.; Harley, P.; Grace, J.; Malhi, Y.; Guenther, A. Effect of drought on isoprene emission rates from leaves of Quercus virginiana Mill. *Atmos. Environ.* **2004**, *38*, 6149−6156.
(58) Sharkey, T. D.; Loreto, F. Water stress, temperature, and light effects on isoprene emission and photosynthesis of Kudzu leaves. *Oecologia* **1993**, *95*, 328−333.
(59) Funk, J. L.; Mak, J. E.; Lerdau, M. T. Stress-induced changes in carbon sources for isoprene production in Populus deltoides. *Plant Cell Environ.* **2004**, *27*, 747−755.
(60) Monson, R. K.; Trahan, N.; Rosenstiel, T. N.; Veres, P.; Moore, D.; Wilkinson, M.; Norby, R. J.; Volder, A.; Tjoelker, M. G.; Briske, D. D.; Karnosky, D. F.; Fall, R. Isoprene emission from terrestrial ecosystems in response to global change: minding the gap between models and observations. *Philos. Trans. R. Soc., A* **2007**, *365*, 1677−1695.
(61) Preethi, B.; Ramya, R.; Patwardhan, S. K.; Mujumdar, M.; Kripalani, R. H. Variability of Indian summer monsoon droughts in CMIP5 climate models. *Clim. Dyn.* **2019**, *53*, 1937−1962.
(62) Mahto, S. S.; Mishra, V. Dominance of summer monsoon flash droughts in India. *Environ. Res. Lett.* **2020**, *15*, No. 104061.
(63) Rasmussen, D. J.; Fiore, A. M.; Naik, V.; Horowitz, L. W.; Schultz, M. G. Surface ozone-temperature relationships in the eastern US: A monthly climatology for evaluating chemistry-climate models. *Atmos. Environ.* **2012**, *47*, 142−153.
(64) Bloomer, B. J.; Stehr, J. W.; Piety, C. A.; Salawitch, R. J.; Dickerson, R. R. Observed relationships of ozone air pollution with temperature and emissions. *Geophys. Res. Lett.* **2009**, *36*, 269−277.
(65) von Schneidemesser, E.; Monks, P. S.; Plass-Duelmer, C. Global comparison of VOC and CO observations in urban areas. *Atmos. Environ.* **2010**, *44*, 5053−5064.
(66) Yue, X.; Unger, N. Fire air pollution reduces global terrestrial productivity. *Nat. Commun.* **2018**, *9*, No. 5413.

https://doi.org/10.1021/acs.est.1c07260
Environ. Sci. Technol. 2022, 56, 3932−3940